crystals

MDPI

Article

Synthesis of Spinel-Hydroxyapatite Composite Utilizing Bovine Bone and Beverage Can

Agus Pramono [1,*], Gerald Ensang Timuda [2,*], Ganang Pramudya Ahmad Rifai [1] and Deni Shidqi Khaerudini [2,*]

[1] Department of Metallurgical Engineering, Sultan Ageng Tirtayasa University, Jl. Jendral Soedirman KM. 3, Cilegon 42435, Banten, Indonesia
[2] Research Center for Physics, National Research and Innovation Agency (BRIN), Building 440-442 Kawasan PUSPIPTEK, Tangerang Selatan 15314, Banten, Indonesia
* Correspondence: agus.pramono@untirta.ac.id (A.P.); gerald.ensang.timuda@brin.go.id (G.E.T.); deni.shidqi.khaerudini@brin.go.id (D.S.K.)

Abstract: Spinel-based hydroxyapatite composite (SHC) has been synthesized utilizing bovine bones as the source of the hydroxyapatite (HAp) and beverage cans as the aluminum (Al) source. The bovine bones were defatted and calcined in the air atmosphere to transform them into hydroxyapatite. The beverage cans were cut and milled to obtain fine Al powder and then sieved to obtain three different particle mesh size fractions: +100#, −140# + 170#, and −170#, or Al particle size of >150, 90–150, and <90 µm, respectively. The SHC was synthesized using the self-propagating intermediate-temperature synthesis (SIS) method at 900 °C for 2 h with (HAp:Al:Mg) ratio of (87:10:3 wt.%) and various compaction pressure of 100, 171, and 200 MPa. It was found that the mechanical properties of the SHC are influenced by the Al particle size and the compaction pressure. Smaller particle size produces the tendency of increasing the hardness and reducing the porosity of the composite. Meanwhile, increasing compaction pressure produces a reduction of the SHC porosity. The increase in the hardness is also observed by increasing the compaction pressure except for the smallest Al particle size (<90 µm), where the hardness instead becomes smaller.

Keywords: hydroxyapatite composite; spinel; beverage cans; bovine bones

Citation: Pramono, A.; Timuda, G.E.; Rifai, G.P.A.; Khaerudini, D.S. Synthesis of Spinel-Hydroxyapatite Composite Utilizing Bovine Bone and Beverage Can. *Crystals* **2022**, *12*, 96. https://doi.org/10.3390/cryst12010096

Academic Editor: Vladislav V. Gurzhiy

Received: 10 December 2021
Accepted: 7 January 2022
Published: 13 January 2022

1. Introduction

Hydroxyapatite is an important biomedical implant material. It is the natural bone's inorganic component [1], and has good osteoconductivity, biocompatibility, and bioactivity, thus making it easily incorporated into the bones [1–3]. However, the utilization of chemically synthesized hydroxyapatite for hard tissue replacement is limited because it is expensive, while a large quantity of material is required [3]. Furthermore, synthesized hydroxyapatite has different physicochemical properties (such as strength and chemical composition) than the natural one, leading to lower biological activity [4,5]. Therefore, extracting hydroxyapatites from biological materials has been considered to provide a cheaper and up-scalable alternative synthesis route, and to obtain physicochemical properties as close as those of the natural hydroxyapatite. Several biological materials have been reported as the source of the hydroxyapatite, such as bovine bone [3,6], fish scale [4,7], snail shell [2,8], and eggshell [9,10]. Bovine bone can be considered a biological waste that needs to be recycled. Therefore, processing it into hydroxyapatite is economically and environmentally beneficial.

To further improve the mechanical properties of hydroxyapatite, it can be synthesized into a composite with metal/alloys [11–14], metal oxides [5,15–17], or polymer [1,18]. The composite of hydroxyapatite (SHC) with a single metal element such as in the Mg/HAp system was considered to combine both advantages of biocompatibility and biodegradability in Mg and bioactivity in HAp [11,14]. Improvement of the mechanical properties, such as hardness and compression strength, has been reported in the Mg/HAp composite

compared to pure HAp [14]. However, the Mg/HAp system is more prone to corrosion than the alloy matrix [11]. Therefore, the addition of other metals as an alloying component was considered to improve the corrosion properties, such as in Mg-Sn/HAp [11] or Mg-Ca/HAp [13]. Similarly, composite of HAp with metal oxides such as ZrO_2, TiO_2, Al_2O_3 [5], or MgO [17] were considered as the reinforcement to improve the HAp's mechanical stability [5]. Furthermore, bio-inert material such as the Al_2O_3 poses no harmful effect on the human body [5].

Several methods to incorporate metals and/or metal oxides into HAp to form a composite have been reported, such as sol-gel [19], reactive spark plasma synthesis [20], stir-assisted squeeze casting [11], and powder metallurgy [13,14]. In this study, the composite of HAp with two metal components, Al and Mg, is reported using a novel approach by the self-propagating intermediate-temperature synthesis (SIS) method. The HAp source is provided by the recycled bovine bone and the Al source is supplied from recycled beverage cans which were reported to contain 93–97% of Al [21–23]. The metal components are prone to oxidation due to the presence of oxygen in the environment during the heating process thus leading to the formation of a HAp-spinel ($MgAl_2O_4$) based composite. The introduction of $MgAl_2O_4$ has been reported to improve the phase stability of HAp during sintering [16]. The effect of Al particle size and compaction pressure on the mechanical properties of the composite is discussed.

2. Materials and Methods

2.1. Bovine Bones Treatment

Bovine bones (leg part) were used as the hydroxyapatite (HAp) source material and were obtained from local markets in Jakarta, Indonesia. The bones were defatted by twice boiling for 2 h, followed by washing under running water, then basking in the Sun for 8 h. The dried bones were then cut into smaller pieces of bones by a grinder and calcined at 850 °C for 2 h both in an inert and air atmosphere for comparison purposes. Afterward, the air-calcined bones were disk milled for 20 s to obtain the HAp powder.

2.2. Aluminum Cans Treatment

Aluminum (Al) and magnesium (Mg) were used as the metal component in the composite. In this study, the Al was provided from recycled beverage cans. The cans were square cut to 1 × 1 cm^2 then disk milled for 15 min with the on:off interval time of 1:2 (min/min), producing Al powder. Its purity content was then characterized by the X-ray fluorescence (XRF, S2 PUMA Bruker). The powder was then sieved with the sieve sizes of 100#, 140#, and 170# to obtain three different particle size fractions of +100#, −140# + 170#, and −170#, respectively, or Al particle size of >150, 90–105, and <90 μm, respectively.

2.3. Self-Propagating Intermediate-Temperature Synthesis (SIS)

A mixture of HAp, Al, and Mg (Merck, 99% purity, particle size 60–300 μm, with the majority at >150 μm, see Figure S1 in Supplementary Information) powders with the ratio of (87:10:3 wt.%) was prepared using a shaker mill for 10 min. The mixture was then pelleted with different compaction pressures of 100, 171, and 200 MPa. The nine different compositions of pellets were prepared from the variation of Al particle sizes and compaction pressures. Afterwards, each pellet was put in the SIS vessel which was then heated at 900 °C for 2 h in an air atmosphere. The SIS vessel is specifically designed so that when undergoing heat treatment in the furnace, the heat propagation can only come from one specific surface instead of from all surfaces in the conventional heat treatment case. In this way, the heat propagation and distribution in the sample became more controllable and homogenous. More detailed information about the SIS method is presented in the Supplementary Information (Figures S2–S4, Table S1).

3. Results and Discussions

The hydroxyapatite composite (SHC) synthesized in this study consists of hydroxyapatite (HAp), aluminum (Al), and magnesium (Mg) as the bio-ceramic matrix, reinforcement, and wetting agent/binder [24–28], respectively. The HAp was extracted from the bovine bones. Figure S5 (Supplementary Information) shows the visual appearance of the defatted bovine bones after calcination in the furnace at 850 °C for 2 h. It can be seen that calcination at 850 °C in an inert condition resulted in burnt and charred bones (Figure S5a, Supplementary Information), indicating the formation of carbon instead of the desired HAp. This is because heating in a low or no oxygen atmosphere can lead to pyrolysis, resulting in carbonization of the bones [29]. On the other hand, the bones that are calcined at 850 °C in an air atmosphere have a white color (Figure S5b, Supplementary Information), indicating the formation of the desired HAp [3,30]. The air-calcined bones also lose their previous stickiness feels, indicating the removal of the remaining fat unable to be removed from the previous defatting process. The air-calcined bones were then crushed in the disk milling to obtain the HAp powder used for the next step of the composite synthesis. Figure S6 (Supplementary Information) shows the photograph of the HAp powders from different batches, showing similar white colors. The particle size distribution of the HAp powder is presented in Figure S1 (Supplementary Information) showing that the majority of the HAp particles have sizes at the range of 90–150 µm, in a similar dimension with the Al powders used in this study.

The XRD of the HAp powders from several batches with similar calcination processes is shown in Figure 1, showing a similar pattern indicating good reproducibility. The unit cell results were also compared with the reference HAp peak (COD 96-901-3628). HAp has a hexagonal crystal structure with the space group of P 63/m and the space group number of 176. It reveals that fully crystalline calcined HAp is observed for all the samples with similar reflection peaks. This is also supported by its small difference of lattice constant (unit cell) after Rietveld refinement of each sample (Table 1), which indicates a good reproducibility. Figure 1b shows the diffraction peaks at a small 2θ angle between 30 and 35°, showing a clearer comparison of the three main peaks of (211), (112), and (300). Three out of four samples show almost similar peaks position. Only the HAp-A sample shows a right-shift of the (211) and (300) peaks, as well as the reduction of the (112) peak. One possible reason for the phenomena is the difference in the actual temperature of the calcination process. Ref. [31] reported similar behavior of the HAp derived from the calcined swine bones. A right-shift of some of the peaks and the disappearance tendency of the (112) peak were observed when the calcination was performed at a lower temperature.

Table 1. The lattice constant of the HAp powders.

Sample	HAp-A	HAp-B	HAp-C	HAp-D	Reference *
a (Å)	9.387	9.425	9.423	9.426	9.421
c (Å)	6.885	6.883	6.883	6.882	6.893

* COD 96-901-3628.

The SEM-EDS of the HAp powder is shown in Figure 2. It can be seen that the distribution of Ca and P are almost similar, indicating the formation of hydroxyapatite. The elemental composition derived from the EDS measurements is presented in Table 2. The Ca/P ratio is at 1.47, slightly smaller than the typical hydroxyapatite at 1.67 [32].

Table 2. Elemental composition of the HAp powder derived from the EDS measurements.

Elements	O	P	Ca	Total
at. %	69.05	12.54	18.41	100.00

Al is the metal used in the composite here as a reinforcement to improve the mechanical properties of the HAp bio-ceramic. In this study, the Al source was taken from recycled beverage cans. The recycling process includes cutting the cans and then crushing them

in the disk milling. After milling, the purity of the crushed powder was characterized using XRF (Table 3). The Al content is at 91.90 ± 1.50%, which is slightly smaller than those reported in the literature (about 93–97% [21–23]). This may come from the paint coating of the can's exterior which was not removed before being recycled, to simplify the recycling process. The impurities are detected in minuscule amounts, where Mn, Si, Fe, and Cu are the four largest impurities percentage at 3.20, 2.80, 1.39, and 0.62%, respectively. Other impurities are less than 0.1% which are relatively negligible. These impurities have been reported to be, instead, intentionally added into HAp for implant materials in many reports to improve the mechanical and biochemical properties of HAp. Mn blended into HAp has been reported to improve the bioactivity of HAp [33]. Mn was also used as a HAp dopant to facilitate its synthesis process and improve its structural and thermal stability [34,35]. Similarly, Fe was also used to dope HAp to induce a superparamagnetic bioactive phase [36], alter its dielectric properties [37], and enhance osteoblast adhesion [35]. Additionally, both Mn and Fe doping show no toxic effect on the osteoblast cell [35]. Si-substituted HAp has also been reported to increase the HAp bioactivity and improve its thermal stability and sinterability [38]. Cu–HAp nanocomposite has also been synthesized to add antibacterial activity with good cytocompatibility [39].

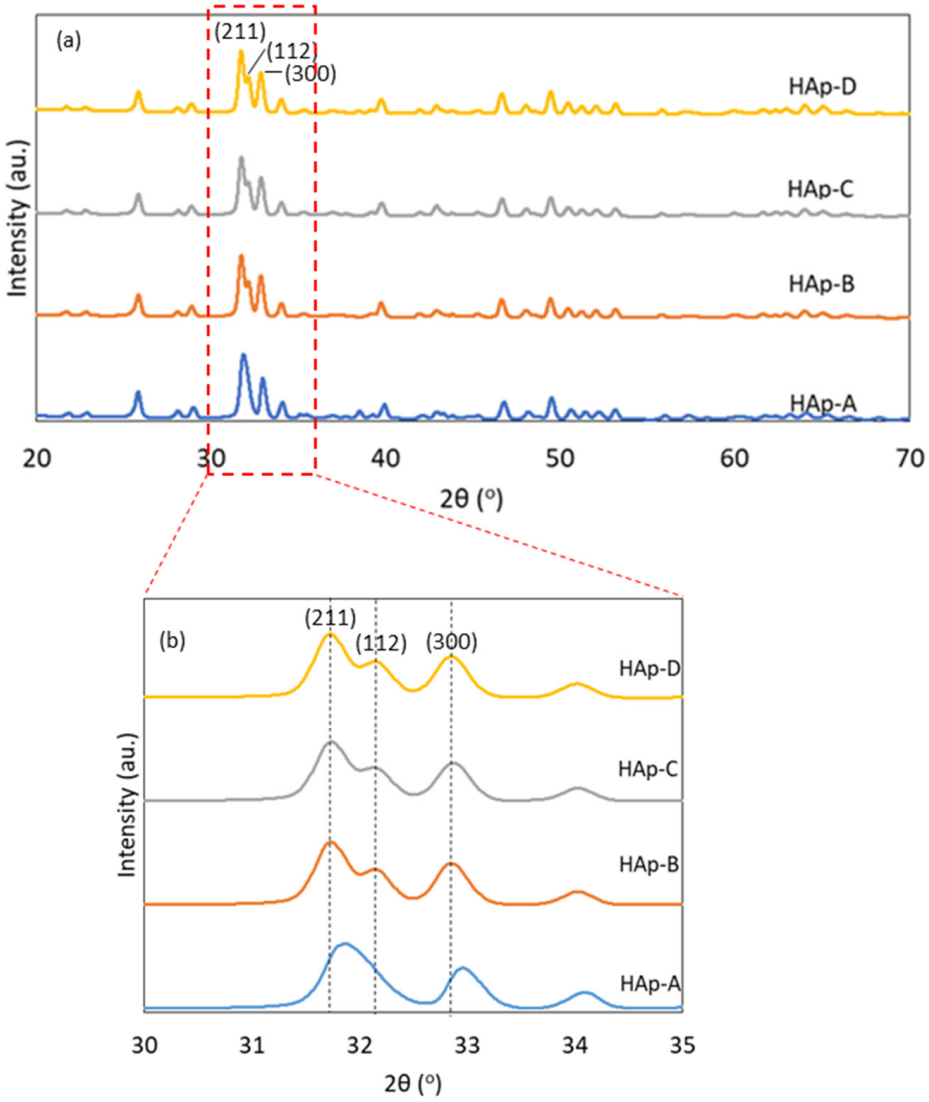

Figure 1. (**a**) X-ray diffractogram and (**b**) expanded X-ray diffractogram of the HAp powders taken from several batches of similar calcination process.

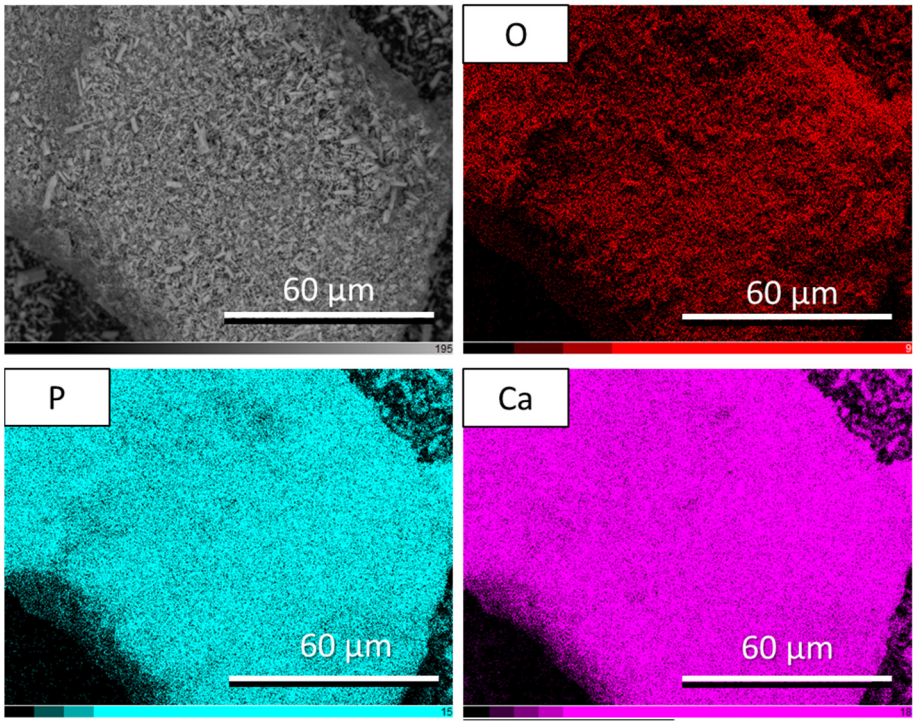

Figure 2. SEM-EDS of the HAp-based bovine bones after calcination in air atmosphere.

Table 3. XRF elemental composition of the Al powder recycled from the beverage can.

Elements	Percentage (%)	Elements	Percentage (%)
Al	91.90 ± 1.50	Ni	0.06 ± 0.02
Mn	3.20 ± 0.40	Zr	0.03 ± 0.03
Si	2.80 ± 0.80	Ti	0.02 ± 0.09
Fe	1.39 ± 0.19	Zn	0.01 ± 0.01
Cu	0.62 ± 0.12		

For application as the reinforcement in the composite, the Al powder was further sieved to obtain a finer and homogenous particle size. The smaller particle size is supposed to give a better homogeneity of the particle's distribution, better bonding among the composite's components, and an increase of the composite's density [40]. Therefore, it is a crucial factor that determines the quality of the composite and is further studied in this report.

For the hydroxyapatite-composite (SHC) synthesis, the HAp, Al, and Mg powders (87:10:3 wt.%) were homogenously mixed which were then pelleted before being heated inside the SIS vessel. The compaction pressure is an important parameter in the SIS method [41]. Here, the effect of the variation of the Al particle size and the compaction pressure on the properties of the SHC is studied.

Figure 3 shows the effect of these variations on the hardness and porosity of the SHC produced. The largest hardness (44.92 HV) is obtained by the smallest particle size (<90 µm). The largest porosity (34.36%) is produced by the biggest particle size (>150 µm). Both with the same compaction pressure of 100 MPa. On the other hand, the smallest hardness (8.36 HV) is produced by the biggest particle size (>150 µm, with the compaction pressure of 100 MPa). Meanwhile, the smallest porosity (19.82%) is obtained by the smallest particle size (<90 µm, with the compaction pressure of 200 MPa). In general, for the same value of compaction pressure, there is a tendency that the smaller the Al particle size produces larger hardness and smaller porosity of the composite. This is in accord with the expectation that the smaller particle size can be homogenously distributed in the mixture and increase the composite's density [40], which is shown by the smaller porosity

and larger hardness. However, if evaluating the value of each Al particle size group, the tendency is not consistent for all cases. For most of the cases, the larger the compaction pressure tends to give larger hardness and smaller porosity. The exception is for the smallest size-fraction (<90 μm) where the larger the compaction pressure instead gives the smaller hardness (dashed lines in Figure 3a). The trend tendency of the porosity, on the other hand, is more consistent (Figure 3b). The reason for the deviation of the hardness trend is unconfirmed at the present but might be related to the formation of the oxides, which will be discussed later. The largest hardness obtained in this study (44.92 HV) is close to those of the human teeth dentin's (46–64 HV [42,43]) and human cortical bone's (40.38 HV [44]). However, its porosity is at 31.12% while the human cortical bone's one needs to be less than 30% [45]. Some samples fulfilled the porosity criteria for the cortical bone in this study such as (90–105 μm) 171 MPa and (<90 μm) 171 MPa with the porosity of 29.45 and 28.58%, respectively, but their hardness values are much lower than the criteria (at 22.15 and 34.52, respectively). However, judging the trend of the hardness and porosity in the (<90 μm) group, it can be projected that the criteria of hardness at around 40 HV with the porosity of less than 30% is possible to be obtained using a compaction pressure between 100 and 171 MPa.

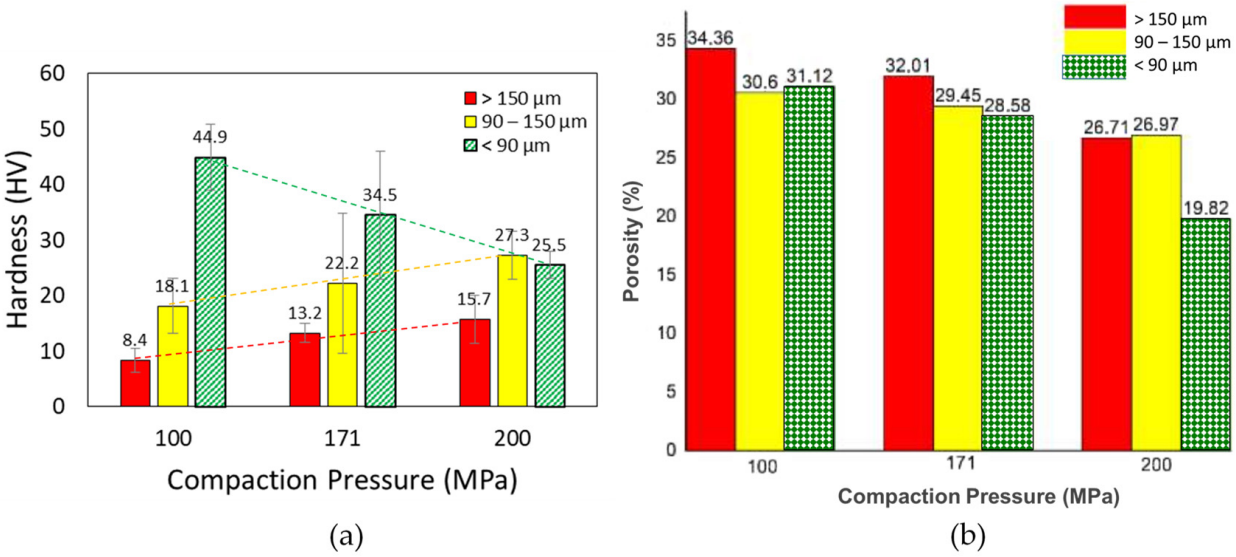

Figure 3. Bar charts of the (**a**) hardness and (**b**) porosity of the hydroxyapatite composite as a function of Al particle size-fraction and compaction pressure. Dashed lines are for a vision guide.

Figure 4 shows the XRD of the SHC made by the compaction pressure at 100 MPa with the Al particle size of <90 and >150 μm. Both samples show the formation of oxides in the form of magnesia (MgO), and spinel ($MgAl_2O_4$) beside the hydroxyapatite. The formation of the oxides is because the SIS heating was performed in a non-vacuum furnace and without flowing an inert gas as well. Therefore, there was air trapped in the SIS vessel which allows oxidation of the metal components. However, for the Al particle size of <90 μm, there are extra alumina (Al_2O_3) peaks detected (Figure 4a).

This indicates that in the case of smaller Al particle size (<90 μm), the oxidation of the Al metal into alumina is easier compared to those of spinel. On the other hand, for bigger Al particle size (>150 μm), the oxidation of Al metal is more favorable toward the spinel formation, as shown by the presence of Al and spinel peaks but in the absence of alumina (Figure 4b). Alumina is a known bio-ceramic for medical applications, such as in dental applications (i.e., orthodontic brackets, dental implants, fixed prostheses, and bone cement filler) [46], or joint replacements [47]. The presence of alumina has also been reported to increase the hardness of a composite [48]. The presence of alumina might be responsible for the increase of the hardness observed from 8.36 to 44.92 HV for >150 and <90 μm, respectively. Another possibility of the increase of hardness is coming from the increase of crystallinity of the HAp [49]. The HAp peak at (112) in the >150 μm sample is

relatively taller compared to the <90 μm one, indicating its higher crystallinity. The higher the HAp crystallinity instead produces a smaller hardness value in this study, opposite to those reported by Ref. [49]. This indicates that the effect of Al_2O_3 formation on the composite's hardness is more dominant.

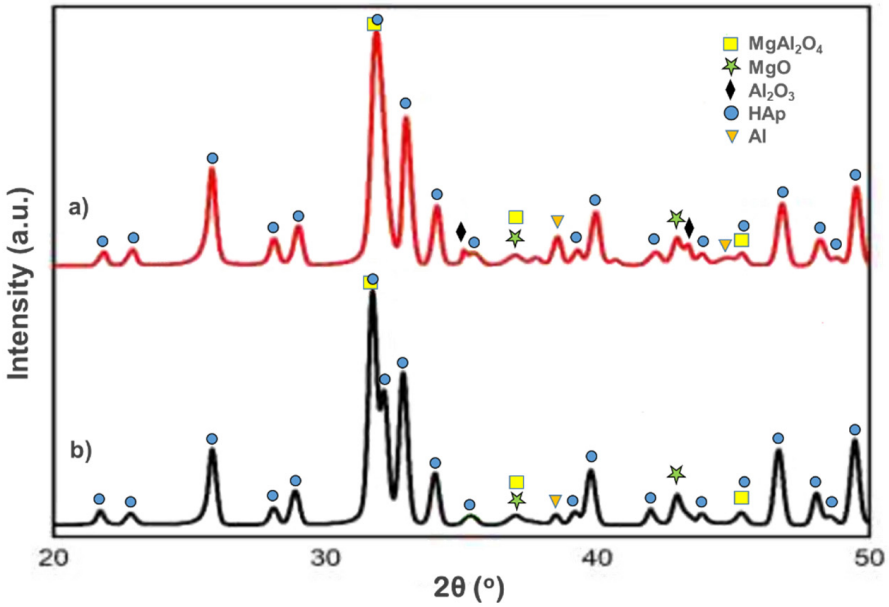

Figure 4. XRD of the hydroxyapatite composite made by compaction pressure of 100 MPa and Al particle size of (**a**) <90 and (**b**) >150 μm.

Figure 5 shows the XRD of the hydroxyapatite composite made using the smaller Al particle size (<90 μm) with different compaction pressures of 100 and 200 MPa. As explained above, for the 100 MPa case, the peaks of alumina and Al metal can be observed (Figure 5b). However, increasing the pressure to 200 MPa completely transforms Al metal into the $MgAl_2O_4$ spinel, as shown in the absence of both alumina and Al metal peaks (Figure 5a). This explains the decrease of the hardness of the 200 MPa sample compared to the 100 MPa one (25.49 and 44.92 HV for 200 and 100 MPa samples, respectively), even though the higher pressure is supposed to increase the density (as shown by the smaller porosity in Figure 3b), which eventually increase the hardness. This indicates that for the hydroxyapatite composite made of smaller Al particle size (<90 μm) in this study, the presence of alumina is crucial in increasing its mechanical properties (hence the hardness). The HAp peak at (112) of the 200 MPa sample is relatively taller than those of the 100 MPa sample, indicating its higher crystallinity. Again, like in the above case, the higher HAp crystallinity instead produces smaller hardness, indicating that the effect of Al_2O_3 formation on the hardness is more dominant.

Figures 6 and 7 show the SEM-EDS pictures of the SHC made by compaction pressure of 100 MPa and Al particle size of <90 and >150 μm, respectively. The Ca and P distribution of the >150 μm sample seems to be better than the <90 μm one. Nevertheless, for each case, the Ca and P have an almost similar distribution, indicating the formation of the hydroxyapatite. The Ca/P ratio for the two samples, calculated from the elemental composition derived from the EDS measurements (Table 4), is almost similar at 1.47 and 1.46 for <90 and >150 μm, respectively, slightly smaller than the typical hydroxyapatite at 1.67 [32]. For both cases, the distribution of Al and Mg were not necessarily overlapping, indicating the formation of other phases besides the spinel $MgAl_2O_4$. This is supporting the XRD result (Figure 4) where the Al and MgO peaks are also observed besides the spinel $MgAl_2O_4$ one.

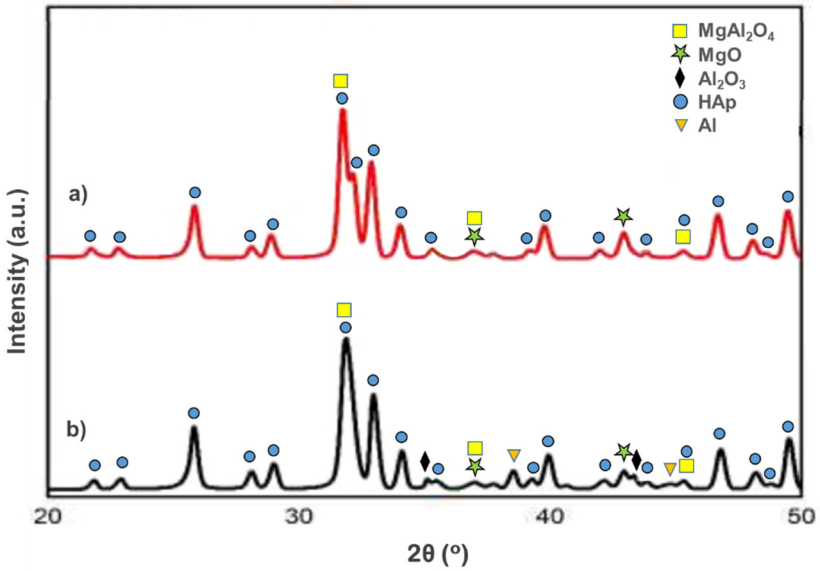

Figure 5. XRD of the hydroxyapatite composite made using Al particle size-fraction of <90 µm and compaction pressure of (**a**) 200 and (**b**) 100 MPa.

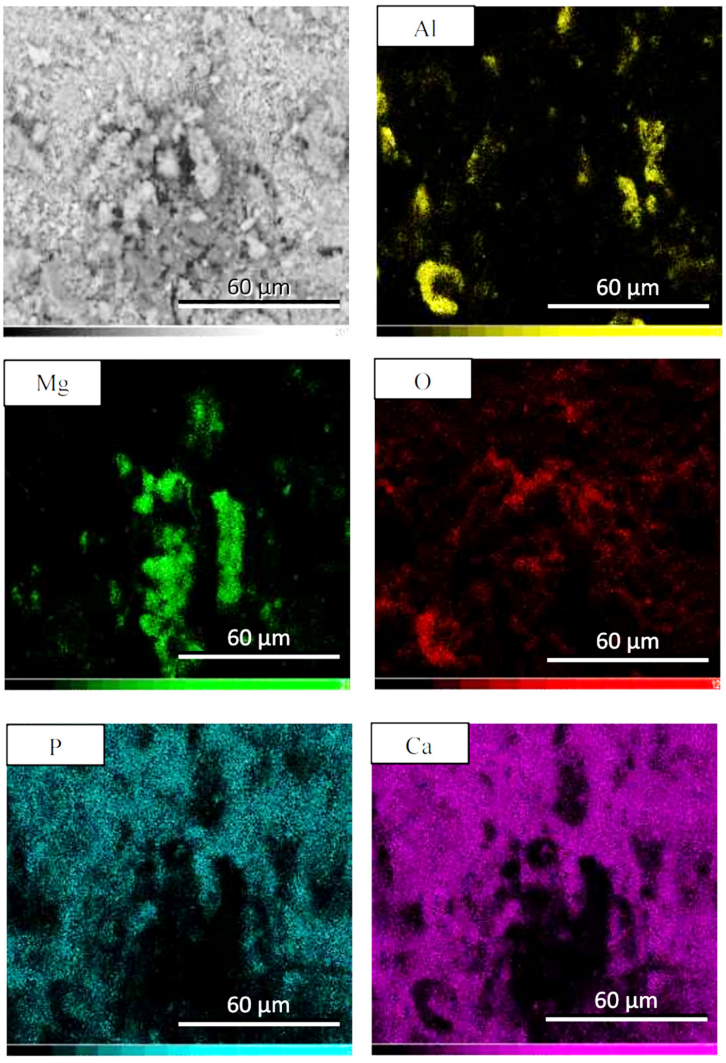

Figure 6. SEM-EDX pictures of the hydroxyapatite composite made by Al particle size of <90 µm with compaction pressure of 100 MPa.

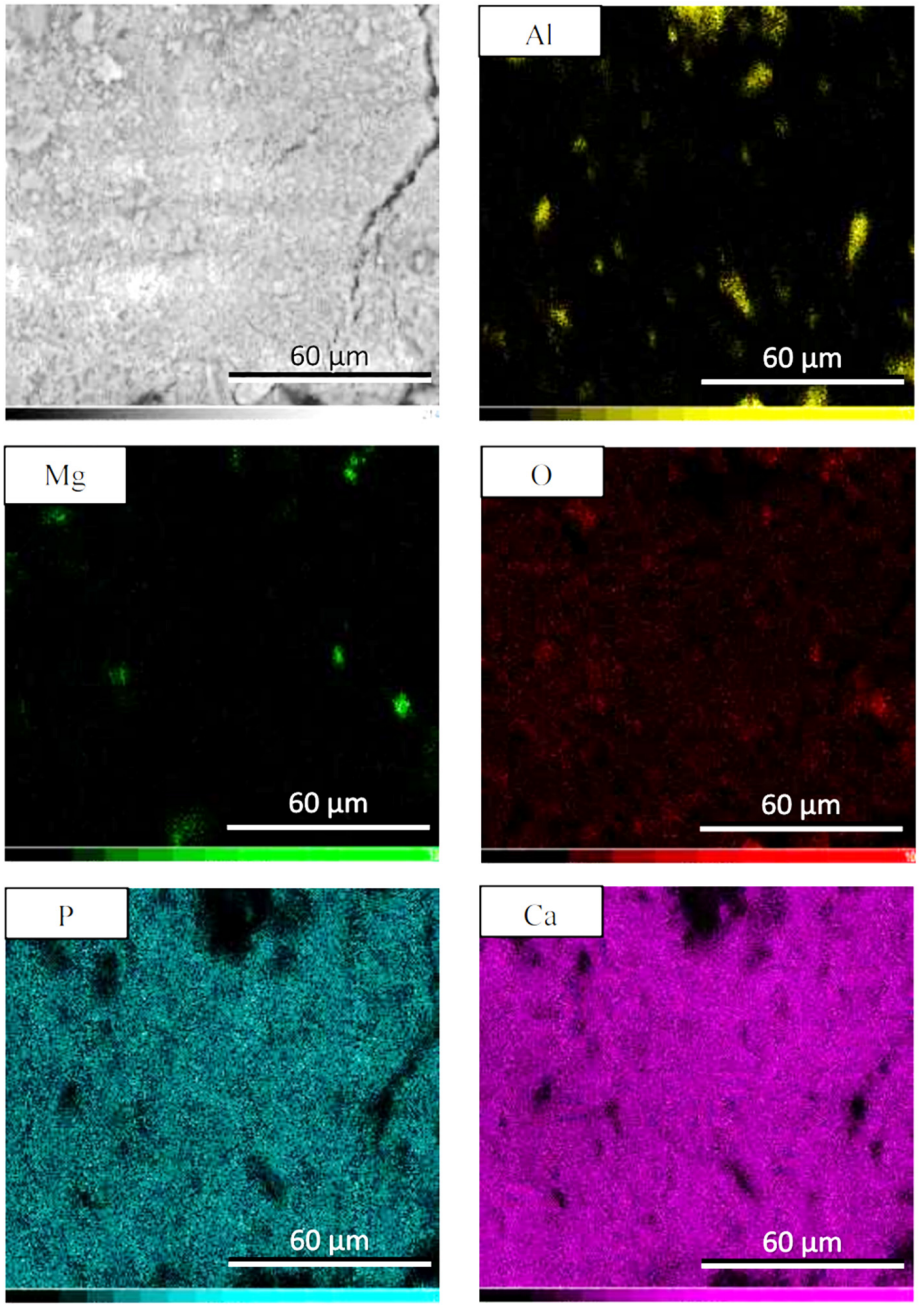

Figure 7. SEM-EDS pictures of the hydroxyapatite composite made by Al size-fraction of >150 µm with compaction pressure of 100 MPa.

Table 4. Elemental composition derived from the EDS measurements of the hydroxyapatite composite made by Al particle size of <90 µm and >150 µm with the compaction pressure of 100 MPa.

Elements	**at. %**	
	<90 µm	**>150 µm**
O	66.75	66.60
Mg	2.47	2.12
Al	2.46	4.22
P	11.45	10.20
Ca	16.87	14.86
Total	100.00	100.00

4. Conclusions

We have successfully synthesized spinel-based hydroxyapatite composite (SHC) using bovine bones and beverage cans as hydroxyapatite and aluminum (Al) metal sources, respectively, using the self-propagating intermediate-temperature synthesis (SIS) method. Aluminum particle size and compaction pressure play important roles in determining the mechanical properties of the SHC. Decreasing the Al particle size tends to increase the hardness and reduce the porosity of the SHC. Increasing compaction pressure also tends to decrease the porosity of the SHC. On the other hand, for the hardness value, the tendency of it to increase as the compaction pressure is increased only applies to the bigger Al particle sizes. For the smallest Al particle size, the higher the compaction pressure instead decreases the hardness value. This is probably related to the presence of the alumina in the smaller pressure which contributes to the improvement of the composite's mechanical properties.

Supplementary Materials: The following supporting information can be downloaded at https://www.mdpi.com/article/10.3390/cryst12010096/s1: Figure S1. Particle size distribution of (a) the synthesized HAp, and (b) Mg powder. Figure S2. Transient thermal distribution of heat flux by SIS heating. Figure S3. The heat flux plots of SIS heating. Figure S4. Results of Taguchi method optimization evaluated by Minitab. Figure S5. Photograph of bovine bones after calcination in (a) inert nitrogen gas, and (b) air atmosphere. Figure S6. Photograph of the HAp powder from different batches. Table S1. Difference between the minimum and maximum temperature of the sample during SIS heating. After cooling down, the hydroxyapatite-composite (SHC) samples in the SIS vessel were taken out then polished by sandpaper and characterized using Archimedes porosity test [24,25], Vickers hardness test (LECO, LM 100 AT, 3 indentations for each sample), X-ray diffraction (XRD, Smart Lab Rigaku, with the source of Cu-Kα), and scanning electron microscopy equipped with Energy X-ray Dispersion Spectroscopy (SEM-EDS, SU-3500 Hitachi, Oxford Instruments Aztech One).

Author Contributions: Conceptualization, D.S.K.; data curation, G.E.T.; formal analysis, G.P.A.R. and D.S.K.; funding acquisition, A.P.; investigation, G.P.A.R. and D.S.K.; methodology, A.P. and D.S.K.; supervision, A.P., G.E.T. and D.S.K.; validation, A.P., G.E.T. and G.P.A.R.; visualization, A.P.; writing—original draft, G.E.T.; writing—review & editing, A.P. and D.S.K. All authors have read and agreed to the published version of the manuscript.

Funding: This research was initiated by Hibah Penelitian Kementrian Pendidikan dan Kebudayaan, part of being funded by Penelitian Terapan Unggulan Perguruan Tinggi (PTUPT), with contract number: B/03/UN43.9/PT.00.03/2020.

Institutional Review Board Statement: Not applicable.

Informed Consent Statement: Not applicable.

Data Availability Statement: Data are contained within the article.

Acknowledgments: Authors acknowledge the Mechanical Materials Metallurgical Laboratory I and II, Engineering Faculty of Sultan Ageng Tirtayasa University and Research Center for Physics, National Research and Innovation Agency (BRIN) for research facilities.

Conflicts of Interest: The authors declare no conflict of interest.

References

1. Wu, S.; Wang, J.; Zou, L.; Jin, L.; Wang, Z.; Li, Y. A Three-Dimensional Hydroxyapatite/ Polyacrylonitrile Composite Scaffold Designed for Bone Tissue Engineering. *RSC Adv.* **2018**, *8*, 1730–1736. [CrossRef]
2. Sari, Y.W.; Rudianto, R.P.; Nuzulia, N.A.; Sukaryo, S.G. Injectable Bone Substitute Synthesized from Mangrove Snail Shell. *J. Med. Phys. Biophys.* **2017**, *4*, 115–121.
3. Odusote, J.K.; Danyuo, Y.; Baruwa, A.D.; Azeez, A.A. Synthesis and Characterization of Hydroxyapatite from Bovine Bone for Production of Dental Implants. *J. Appl. Biomater. Funct. Mater.* **2019**, *17*, 2280800019836829. [CrossRef]
4. Pon-On, W.; Suntornsaratoon, P.; Charoenphandhu, N.; Thongbunchoo, J.; Krishnamra, N.; Tang, I.M. Hydroxyapatite from Fish Scale for Potential Use as Bone Scaffold or Regenerative Material. *Mater. Sci. Eng. C* **2016**, *62*, 183–189. [CrossRef]
5. Vignesh Raj, S.; Rajkumar, M.; Meenakshi Sundaram, N.; Kandaswamy, A. Synthesis and Characterization of Hydroxyapatite/Alumina Ceramic Nanocomposites for Biomedical Applications. *Bull. Mater. Sci.* **2018**, *41*, 93. [CrossRef]

6. Budiatin, A.S.; Gani, M.A.; Samirah; Ardianto, C.; Raharjanti, A.M.; Septiani, I.; Putri, N.P.K.P.; Khotib, J. Bovine Hydroxyapatite-Based Bone Scaffold with Gentamicin Accelerates Vascularization and Remodeling of Bone Defect. *Int. J. Biomater.* **2021**, *2021*, 5560891. [CrossRef] [PubMed]
7. Huang, Y.; Hsiao, P.; Chai, H. Hydroxyapatite Extracted from Fish Scale: Effects on MG63 Osteoblast-like Cells. *Ceram. Int.* **2011**, *37*, 1825–1831. [CrossRef]
8. Kumar, G.S.; Sathish, L.; Govindan, R.; Girija, E.K. Utilization of Snail Shells to Synthesise Hydroxyapatite Nanorods for Orthopedic Applications. *RSC Adv.* **2015**, *5*, 39544–39548. [CrossRef]
9. Abdulrahman, I.; Tijani, H.I.; Mohammed, B.A.; Saidu, H.; Yusuf, H.; Ndejiko Jibrin, M.; Mohammed, S. From Garbage to Biomaterials: An Overview on Egg Shell Based Hydroxyapatite. *J. Mater.* **2014**, *2014*, 802467. [CrossRef]
10. Kattimani, V.; Lingamaneni, K.P.; Chakravarthi, P.S.; Sampath Kumar, T.S.; Siddharthan, A. Eggshell-Derived Hydroxyapatite: A New Era in Bone Regeneration. *J. Craniofac. Surg.* **2016**, *27*, 112–117. [CrossRef] [PubMed]
11. Radha, R.; Sreekanth, D. Mechanical and Corrosion Behaviour of Hydroxyapatite Reinforced Mg-Sn Alloy Composite by Squeeze Casting for Biomedical Applications. *J. Magnes. Alloy.* **2020**, *8*, 452–460. [CrossRef]
12. Witte, F.; Feyerabend, F.; Maier, P.; Fischer, J.; Störmer, M.; Blawert, C.; Dietzel, W.; Hort, N. Biodegradable Magnesium-Hydroxyapatite Metal Matrix Composites. *Biomaterials* **2007**, *28*, 2163–2174. [CrossRef]
13. Lim, P.N.; Lam, R.N.; Zheng, Y.F.; Thian, E.S. Magnesium-Calcium/Hydroxyapatite (Mg-Ca/HA) Composites with Enhanced Bone Differentiation Properties for Orthopedic Applications. *Mater. Lett.* **2016**, *172*, 193–197. [CrossRef]
14. Del Campo, R.; Savoini, B.; Muñoz, A.; Monge, M.A.; Garcés, G. Mechanical Properties and Corrosion Behavior of Mg-HAP Composites. *J. Mech. Behav. Biomed. Mater.* **2014**, *39*, 238–246. [CrossRef] [PubMed]
15. Li, J.; Fartash, B.; Hermansson, L. Hydroxyapatite-Alumina Composites and Bone-Bonding. *Biomaterials* **1995**, *16*, 417–422. [CrossRef]
16. Yoon, H.J.; Yoon, J.H.; Park, S.H.; Lee, M.H.; Han, J.S.; Kim, D.J. The Role of MgAl2O4 Powder Packing on Phase Stability of Hydroxyapatite during Sintering. *J. Am. Ceram. Soc.* **2015**, *98*, 1787–1793. [CrossRef]
17. Sreekanth, D.; Rameshbabu, N. Development and Characterization of MgO/Hydroxyapatite Composite Coating on AZ31 Magnesium Alloy by Plasma Electrolytic Oxidation Coupled with Electrophoretic Deposition. *Mater. Lett.* **2012**, *68*, 439–442. [CrossRef]
18. Wei, G.; Ma, P.X. Structure and Properties of Nano-Hydroxyapatite/Polymer Composite Scaffolds for Bone Tissue Engineering. *Biomaterials* **2004**, *25*, 4749–4757. [CrossRef]
19. Papynov, E.K.; Shichalin, O.O.; Apanasevich, V.I.; Plekhova, N.G.; Buravlev, I.Y.; Zinoviev, S.V.; Mayorov, V.Y.; Fedorets, A.N.; Merkulov, E.B.; Shlyk, D.K.; et al. Synthetic Nanostructured Wollastonite: Composition, Structure and "in Vitro" Biocompatibility Investigation. *Ceram. Int.* **2021**, *47*, 22487–22496. [CrossRef]
20. Papynov, E.K.; Shichalin, O.O.; Buravlev, I.Y.; Portnyagin, A.S.; Belov, A.A.; Maiorov, V.Y.; Skurikhina, Y.E.; Merkulov, E.B.; Glavinskaya, V.O.; Nomerovskii, A.D.; et al. Reactive Spark Plasma Synthesis of Porous Bioceramic Wollastonite. *Russ. J. Inorg. Chem.* **2020**, *65*, 263–270. [CrossRef]
21. Risonarta, V.Y.; Anggono, J.; Suhendra, Y.M.; Nugrowibowo, S.; Jani, Y. Strategy to Improve Recycling Yield of Aluminium Cans. *E3S Web Conf.* **2019**, *130*, 01033. [CrossRef]
22. Begum, S. Recycling of Aluminum from Aluminum Cans. *J. Chem. Soc. Pakistan* **2013**, *35*, 1490–1493.
23. Akrom, M.; Marwoto, P. Sugianto Pembuatan Mmc Berbasis Teknologi Metalurgi Serbuk Dengan Bahan Baku Aluminium Dari Limbah Kaleng Minuman Dan Aditif Abu Sekam Padi. *J. Pendidik. Fis. Indones.* **2010**, *6*, 14–19.
24. Slotwinski, J.A.; Garboczi, E.J.; Hebenstreit, K.M. Porosity Measurements and Analysis for Metal Additive Manufacturing Process Control. *J. Res. Natl. Inst. Stand. Technol.* **2014**, *119*, 494–528. [CrossRef] [PubMed]
25. Converse, G.L.; Conrad, T.L.; Merrill, C.H.; Roeder, R.K. Hydroxyapatite Whisker-Reinforced Polyetherketoneketone Bone Ingrowth Scaffolds. *Acta Biomater.* **2010**, *6*, 856–863. [CrossRef] [PubMed]
26. Poovazhagan, L.; Rajkumar, K.; Saravanamuthukumar, P.; Javed Syed Ibrahim, S.; Santhosh, S. Effect of Magnesium Addition on Processing the Al-0.8 Mg-0.7 Si/SiCp Metal Matrix Composites. *Appl. Mech. Mater.* **2015**, *787*, 553–557. [CrossRef]
27. Sangghaleh, A.; Halali, M. Effect of Magnesium Addition on the Wetting of Alumina by Aluminium. *Appl. Surf. Sci.* **2009**, *255*, 8202–8206. [CrossRef]
28. Hasanah, I.U.; Fadhillah, M.F.; Putra, Y.V. Fabrication and Characterization of Aluminum Matrix Composite (AMCs) Reinforced Graphite by Stir Casting Method for Automotive Application. *Mater. Sci. Forum* **2020**, *988*, 17–22.
29. Dahi, E. Optimisation of Bone Char Production Using the Standard Defluoridation Capacity Procedure. *Fluoride* **2015**, *48*, 29–36.
30. Fadhilah, N.; Irhamni, I.; Jalil, Z. Synthesis of Natural Hydroxyapatite from Aceh's Bovine Bone. *J. Aceh Phys. Soc.* **2016**, *5*, 19–21.
31. Londoño-Restrepo, S.M.; Herrera-Lara, M.; Bernal-Alvarez, L.R.; Rivera-Muñoz, E.M.; Rodriguez-García, M.E. In-Situ XRD Study of the Crystal Size Transition of Hydroxyapatite from Swine Bone. *Ceram. Int.* **2020**, *46*, 24454–24461. [CrossRef]
32. Singh, T.P.; Singh, H.; Singh, H. Characterization of Thermal Sprayed Hydroxyapatite Coatings on Some Biomedical Implant Materials. *J. Appl. Biomater. Funct. Mater.* **2014**, *12*, 48–56. [CrossRef]
33. Mahabole, M.; Bahir, M.; Khairnar, R. Mn Blended Hydroxyapatite Nanoceramic: Bioactivity, Dielectric and Luminescence Studies. *J. Biomim. Biomater. Tissue Eng.* **2013**, *18*, 43–59. [CrossRef]
34. Paluszkiewicz, C.; Ślósarczyk, A.; Pijocha, D.; Sitarz, M.; Bućko, M.; Zima, A.; Chróścicka, A.; Lewandowska-Szumieł, M. Synthesis, Structural Properties and Thermal Stability of Mn-Doped Hydroxyapatite. *J. Mol. Struct.* **2010**, *976*, 301–309. [CrossRef]

35. Li, Y.; Widodo, J.; Lim, S.; Ooi, C.P. Synthesis and Cytocompatibility of Manganese (II) and Iron (III) Substituted Hydroxyapatite Nanoparticles. *J. Mater. Sci.* **2012**, *47*, 754–763. [CrossRef]
36. Panseri, S.; Cunha, C.; D'Alessandro, T.; Sandri, M.; Giavaresi, G.; Marcacci, M.; Hung, C.T.; Tampieri, A. Intrinsically Superparamagnetic Fe-Hydroxyapatite Nanoparticles Positively Influence Osteoblast-like Cell Behaviour. *J. Nanobiotechnol.* **2012**, *10*, 32. [CrossRef] [PubMed]
37. Kaygili, O.; Dorozhkin, S.V.; Ates, T.; Al-Ghamdi, A.A.; Yakuphanoglu, F. Dielectric Properties of Fe Doped Hydroxyapatite Prepared by Sol-Gel Method. *Ceram. Int.* **2014**, *40*, 9395–9402. [CrossRef]
38. Bianco, A.; Cacciotti, I.; Lombardi, M.; Montanaro, L. Si-Substituted Hydroxyapatite Nanopowders: Synthesis, Thermal Stability and Sinterability. *Mater. Res. Bull.* **2009**, *44*, 345–354. [CrossRef]
39. Hadidi, M.; Bigham, A.; Saebnoori, E.; Hassanzadeh-Tabrizi, S.A.; Rahmati, S.; Alizadeh, Z.M.; Nasirian, V.; Rafienia, M. Electrophoretic-Deposited Hydroxyapatite-Copper Nanocomposite as an Antibacterial Coating for Biomedical Applications. *Surf. Coat. Technol.* **2017**, *321*, 171–179. [CrossRef]
40. Oh, S.-T.; Sekino, T.; Niihara, K. Effect of Particle Size Distribution and Mixing Homogeneity on Microstructure and Strength of Alumina/Copper Composites. *Nanostruct. Mater.* **1998**, *10*, 327–332. [CrossRef]
41. Halverson, D.C.; Pyzik, A.J.; Aksay, I.A.; Snowden, W.E. Processing of Boron Carbide-Aluminum Composites. *J. Am. Ceram. Soc.* **1989**, *72*, 775–780. [CrossRef]
42. Del Gutiérrez-Salazar, M.P.; Reyes-Gasga, J. Microhardness and Chemical Composition of Human Tooth. *Mater. Res.* **2003**, *6*, 367–373. [CrossRef]
43. Craıg, R.G.; Peyton, F.A. The Micro-Hardness of Enamel and Dentin. *J. Dent. Res.* **1958**, *37*, 661–668. [CrossRef]
44. Pramanik, S.; Agarwal, A.K.; Rai, K.N. Development of High Strength Hydroxyapatite for Hard Tissue Replacement. *Trends Biomater. Artif. Organs* **2005**, *19*, 45–49.
45. Keaveny, T.M.; Morgan, E.F.; Yeh, O.C. Bone Mechanics. In *Standard Handbook of Biomedical Engineering and Design*; Kutz, M., Ed.; The McGraw-Hill Companies, Inc.: New York, NY, USA, 2004; pp. 8.1–8.23, ISBN 9780071356374.
46. Al-Sanabani, F.A.; Madfa, A.A.; Al-Qudaini, N. Alumina Ceramic for Dental Applications: A Review Article. *Am. J. Mater. Res.* **2014**, *1*, 26–34.
47. Piconi, C.; Maccauro, G.; Muratori, F.; Brach Del Prever, E. Alumina and Zirconia Ceramics in Joint Replacements. *J. Appl. Biomater. Biomech.* **2003**, *1*, 19–32.
48. Latief, F.H.; Chafidz, A.; Junaedi, H.; Alfozan, A.; Khan, R. Effect of Alumina Contents on the Physicomechanical Properties of Alumina (Al2O3) Reinforced Polyester Composites. *Adv. Polym. Technol.* **2019**, *2019*, 5173537. [CrossRef]
49. Yanagisawa, K.; Zhu, K.; Fujino, T.; Onda, A. Preparation of Hydroxyapatite Ceramics by Hydrothermal Hot-Pressing Technique. *Key Eng. Mater.* **2006**, *309–311*, 57–60. [CrossRef]